

Topological Structure in the $SU(2)$ Vacuum ¹

Thomas DeGrand, Anna Hasenfratz, and Tamás G. Kovács
Department of Physics
University of Colorado, Boulder CO 80309-390

September 2018

Abstract

We study the topological content of the vacuum of $SU(2)$ pure gauge theory using lattice simulations. We use a smoothing process based on the renormalization group equation which removes short distance fluctuations but preserves long distance structure. The action of the smoothed configurations is dominated by instantons, but they still show an area law for Wilson loops with a string tension equal to the string tension on the original configurations. Yet it appears that instantons are not directly responsible for confinement. The average radius of an instanton is about 0.2 fm, at a density of about 2 fm^{-4} . This is a much smaller average size than other lattice studies have indicated. The instantons appear not to be randomly distributed in space, but are clustered.

¹Work supported in part by NSF Grant PHY-9023257 and U. S. Department of Energy grant DE-FG02-92ER-40672

1 Introduction

An important ingredient in the physics of the strong interaction is the influence of topology on dynamics. Based on phenomenological models, it has been argued that instantons are largely responsible for the low energy hadron and glueball spectrum [1, 2]. Instanton liquid models attempt to reproduce the topological content of the QCD vacuum and conclude that hadronic correlators in the instanton liquid show all the important properties of the corresponding full QCD correlators. These models appear to capture the essence of the QCD vacuum, but their derivations involve a number of uncontrolled approximations and phenomenological parameters.

Another example of this connection is the $U(1)$ problem of QCD, whose resolution may involve instanton effects [3]. In the large- N_c limit the mass of the η' is related to the topological susceptibility χ_t through the Witten-Veneziano formula[4]

$$m_{\eta'}^2 + m_{\eta}^2 - 2m_K^2 = 2N_f\chi_t/f_{\pi}^2. \quad (1)$$

While the precise validity of this formula is unclear to us, it indicates the dynamical role of instantons in QCD.

Lattice methods are the only ones we presently have, which might address this connection. Individual instantons can be identified only on smooth enough configurations therefore we perform a smoothing process on the gauge fields which substantially reduces short range fluctuations, but, as we prove and show explicitly, preserves long distance physics. The smoothed configurations show an area law for Wilson loops with a string tension equal to the string tension on the original configurations. We find that the action of these smoothed configurations is dominated by instantons, though tests we perform show that instantons are not directly responsible for confinement.

Our goal in this paper is to study the topological structure of the pure $SU(2)$ gauge vacuum. Our method allows us to identify and study the properties of individual instantons on the lattice whose radius is as small as one lattice spacing. We find that the vacuum is filled with instantons whose average radius is about 0.2 fm, at a density of about 2 fm^{-4} . This is a much smaller average size than other lattice studies have indicated [5, 6]. The instantons appear not to be randomly distributed in space, but are clustered.

1.1 Topology on the lattice

Lattice studies of topology suffer from the presence of lattice artifacts. They can arise both from the form of the lattice action and from the choice of lattice operator used to define and measure topological charge. A lattice action is, in general, not scale invariant, i.e. the action of a smooth continuum instanton can depend on its size. Difficulties also arise because the topological charge is not conserved on the lattice. When the size of an instanton becomes small compared to the lattice spacing, the instanton charge operator will miss it, it "falls through" the lattice. If the size scale of physically relevant instantons is smaller than the size scale at which the lattice simulation supports them, one's predictions will exhibit scaling violations.

Fixed point actions allow us, in principle, to solve the first of these problems. Predictions of physical observables computed from a lattice action and lattice operators which live on the renormalized trajectory (RT) of some renormalization group transformation (RGT) do not depend on the lattice spacing, they are free of lattice artifacts. A recent series of papers [7, 8, 9, 10] has shown how to find a fixed point (FP) action for asymptotically free theories, with explicit examples for spin and gauge models. FP actions share the scaling properties of the RT (through one-loop quantum corrections) and as such may be taken as a first approximation to a RT.

FP actions also offer a way to define a topological charge operator on the lattice, through the RGT equation itself. Suppose we have a configuration of lattice variables $\{V\}$. We will refer to this configuration as coarse. We want to determine the topological properties of $\{V\}$ by mapping it onto a fine configuration $\{U\}$ (defined on a lattice with half the lattice spacing or with 2^4 times the original number of lattice points), which has the same topology as $\{V\}$ but is smooth enough that the standard (geometrical or algebraic) definition of the charge operators work. Such a mapping is possible through the steepest descent FP equation

$$S^{FP}(V) = \min_{\{U\}} (S^{FP}(U) + \kappa T(U, V)), \quad (2)$$

where $T(U, V)$ is the blocking kernel and the parameter κ determines the "stiffness" of the transformation [7, 8, 9, 10].

The fine configuration has the following properties:

1) The blocking kernel $T(U, V)$ is positive-definite, therefore the action on the fine lattice is always equal to or smaller than the action on the coarse lattice, $S^{FP}(U) \leq S^{FP}(V)$.

2) The configuration $\{U\}$ blocks into $\{V\}$ under an RGT step. This statement is correct statistically for arbitrary RGT and becomes exact if $\kappa = \infty$. That justifies referring to the transformation Eqn. 2 as inverse blocking.

3) As a consequence of 2), the long distance, physically relevant properties of $\{U\}$ and $\{V\}$ are identical. In particular, if a correlation length can be defined on a set of coarse lattices, then the correlation length on the fine lattices, constructed by inverse blocking, will be the same as on the coarse lattices, when measured in physical units. In addition to the physical, long distance structure, the fine configuration $\{U\}$ exhibits a peculiar staggered short range structure. This does not change its physical properties but requires special care in measuring the spectrum. We will discuss this point in detail in Section 2.4.

4) The topological properties of $\{U\}$ and $\{V\}$ are identical, at least for instantons that are larger than some fixed radius, ρ_c .

Neither the blocking nor the inverse blocking transformations can create new instantons. The blocking averages over small distance fluctuations, and the inverse blocking finds the minimum of the action constrained by the blocking kernel. None of them allows the short scale fluctuations necessary for creating a small instanton.

A coarse configuration that is topologically trivial will inverse block into a configuration with lower action, and after many levels of inverse blocking the action on the finest lattice will go to zero.

Next consider a smooth continuum instanton configuration. As it was argued in [7], if $\{V\}$ is a solution of the classical equations of motion, so that $\delta S^{FP}(V)/\delta V = 0$, then Eqn. 2 says that $\delta S^{FP}(U)/\delta U = 0$: the configuration on the fine lattice is also a solution to the classical equations of motion, $S^{FP}(V) = S^{FP}(U) = S_I$ i.e. $\{U\}$ is also a continuum instanton configuration. (The opposite is not necessarily true, since small instantons with radius less than ρ_c of the fine configuration could disappear after an RGT.) The same is true for continuum multi-instanton configurations. (When we describe multi-instanton configurations, we will frequently refer to both instantons and anti-instanton as instantons.)

For configurations consisting of instantons/anti-instanton plus fluctuations, a similar argument works. The inverse blocking will not create new instantons; rather, it will decrease the action by smoothing out fluctuations. Since the resulting fine configuration blocks back to the original coarse configuration, it has to have all the topology of the coarse configuration.

The size of the instantons grows by a factor of two under the inverse blocking

but their orientation and location is unchanged. After repeated application of the transformation, the action will approach S_I times the total number of topological objects on the lattice. Thus we can define the topological charge of a configuration by first inverse blocking it to a sufficiently smooth configuration and then measuring the charge with any appropriate operator on the fine lattice.

The preceding paragraphs involved questions of principle. The extent to which they can be achieved in practice depends on our ability to construct a good approximate FP action. In our earlier papers [11, 12] on this subject we found an approximate FP action for SU(2) pure gauge theory, subjected it to scaling tests, and computed the topological susceptibility. We saw that it scaled (within the uncertainties of our simulations) for lattice spacings less than about 0.2 fm, at a value of about $\chi_t^{1/4} = 235$ MeV. We have also presented some preliminary measurements of the temperature dependence of the susceptibility [13].

In this paper we present a new FP action with greatly improved scale invariance and study its topological properties. In Section 2 we introduce the procedures necessary to carry out the calculations. In Section 3 we describe the properties of instantons. Our conclusions are given in Section 4.

2 Methodology

2.1 Construction of an Approximate FP Action

The continuum (tree level) action of QCD is scale invariant, i.e. instantons of different size have the same action. This scale invariance is broken by the lattice cutoff, and the way this happens may be crucial to the continuum limit. The cutoff mainly influences small instantons with sizes around the lattice spacing. If the action of these instantons decreases with their size (as is the case e.g. with the Wilson action) then it can happen that in the continuum limit topological observables will be dominated by small instantons near the cutoff and scaling for these observables will be lost. This was first pointed out in the context of 2d spin models in [14, 15] and in gauge theories in [16, 17]. For a recent discussion of some related questions in Yang-Mills theories see [18].

Topological charge operators can only detect instantons above a certain size, the size cutoff usually being of the order of the lattice spacing. If this cutoff is above the size of the overabundant small instantons, then they will not be observed in topological measurements. That does not mean, however, that they

can be neglected. Their presence can affect the scaling of spectral quantities and cause scaling violations.

A classically perfect action is scale invariant by construction. In Ref. [11] we presented a many-parameter FP action for SU(2) pure gauge theory which satisfied our requirement that $S/S_I \geq 1$ for all charged configurations, and $S/S_I = 1$ for all smooth configurations with topological charge $Q = 1$. This action was too unwieldy to use in simulations. We used two loops, the plaquette and the link-6 twisted loop $(x, y, z, -x, -y, -z)$ to construct an approximate FP action. This approximate action reproduced the FP action value within a couple of percent for Monte Carlo configurations generated at large correlation length but was not scale invariant for smooth instantons. In fact, it was only slightly better than the Wilson action. However, it did satisfy $S/S_I > 6/11$, so that the entropic bound against overproducing dislocations was not violated. We argued that this softer constraint should be adequate for practical calculations. However, in his studies of the CP^3 model [19], Burkhalter saw scale violations from the use of an action similar to ours, and in principle this action should also show scale violations at large lattice spacing as discussed above. In this paper we present an approximate FP action where scale violations are greatly reduced.

The two loops used in Ref. [12] are not sufficient to create a scale invariant action. In our calculation we considered all loops with length less or equal than 8 which fit into a 2^4 hypercube. Among these 28 loops we found that one, the perimeter-eight $(x, y, -x, -y, z, t, -z, -t)$ loop, is essential for constructing a scale invariant action.

Our new approximate FP action consists of four powers of three loops, the plaquette, the perimeter-six loop $(x, y, z, -x, -y, -z)$, and the perimeter-eight loop $(x, y, -x, -y, z, t, -z, -t)$

$$S(V) = c_0 + \frac{1}{N_c} \sum_C (c_1(C)(N_c - \text{Tr}(V_C)) + c_2(C)(N_c - \text{Tr}(V_C))^2 + \dots) \quad (3)$$

with coefficients tabulated in Table 1. It is designed to fit “typical” gauge field configurations in the range $aT_c = 1/3$ to $1/6$, and, in addition, to preserve the scale invariance of pure isolated instanton configurations.

The constant term c_0 in the action is an unusual term, but it is necessary to fit the FP equation Eqn. 2 in the small correlation length range with a few parameters. If we were to attempt to find a parameterization of the FP action valid for larger correlation length, the coefficient c_0 would change and eventually would approach zero as $\beta \rightarrow \infty$. The $c_1 - c_3$ coefficients in Eqn. 3 are normalized such that $S - c_0$ has the correct continuum limit and in a

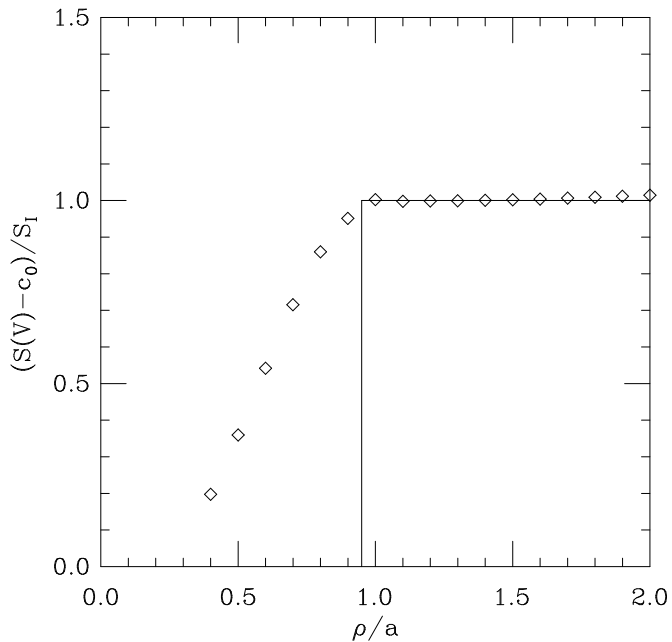


Figure 1: Action vs. instanton radius for the SU(2) action of Table 1.

MC simulation c_0 is clearly irrelevant. To produce instantons with the correct weight the action should give S_I above the vacuum for smooth single instanton configurations. Fig. 1 shows $(S(V) - c_0)/S_I$ vs. instanton radius for a set of smooth instanton configurations. The action indeed scales within a few percent even for small radius instantons.

We have not subjected the SU(2) action to a detailed scaling test (test of the variation of a dimensionless ratio of dimensionful observables with lattice spacing) and we do not know if it has better scaling properties than the action used in Ref. [12] for spectral quantities. However if instantons are as important as the instanton liquid models predict, one would expect improved scaling behavior at least for the glueballs.

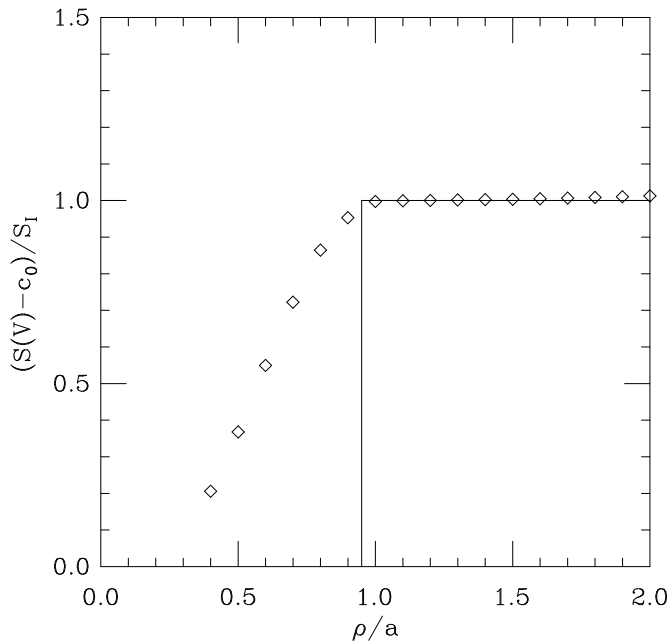


Figure 2: Action vs. instanton radius for the SU(3) action of Table 2.

We have also constructed an SU(3) action with the same operators. We fit “typical” SU(3) Monte Carlo configurations and a set of SU(2) instantons. The analog picture of Fig. 1 is shown in Fig. 2, and a table of the parameter values is given in Table 2. We have not done any detailed scaling tests of this action either. Preliminary values for the critical couplings for deconfinement are near $\beta = 2.38, 2.85$ and 3.05 at $N_t = 2, 3$, and 4 .

These actions are unwieldy to simulate. The problem is the high multiplicity of the perimeter-eight loop (96 distinct paths). The cost of these actions, compared to the standard Wilson action, is a ratio of about 225 per link update. Unfortunately no other loop would produce even approximately similar scale invariance. However, since all the configuration generation is done on small

Table 1: Couplings of the few-parameter FP action for SU(2) pure gauge theory.

operator	c_1	c_2	c_3	c_4	$c_0 = -0.683$
c_{plaq}	.9225	.1804	.0691	-.0194	
c_{6-link}	-.1843	.1408	-.0264	.0047	
c_{8-link}	.0485	-.0238	.0090	.0026	

Table 2: Couplings of the few-parameter FP action for SU(3) pure gauge theory.

operator	c_1	c_2	c_3	c_4	$c_0 = -1.669$
c_{plaq}	2.3350	-.4767	.2465	-.0207	
c_{6-link}	-.2391	.0565	.0305	-.0059	
c_{8-link}	.0181	-.0059	-.0107	.0016	

lattices, generating configurations is a small part of the computational burden, which we are willing to sacrifice to the principle that the action should produce instantons without scale violations.

2.2 An ‘‘Algebraic’’ Topological Charge Operator

In this section we first discuss the main problem arising in connection with the measurement of the topological charge on the lattice. Then we describe how we deal with it and also present the details of our algebraic charge operator.

The difficulty is connected to the fact that a topological charge can be assigned unambiguously only to continuous field configurations living in a continuum space-time. In order to be able to assign a topological charge to a lattice configuration, we first have to choose an interpolation which maps the lattice configuration to a continuum configuration. This interpolation is usually not unique and different interpolations can lead to different topological charge assignments. If the configuration corresponds to a FP action, Eqn. 2 defines this interpolation uniquely for the given FP action. (Different FP actions can have different interpolations and, especially for small instantons, might find different charge on the same coarse configuration.) If the configuration does not correspond to a FP action but to a renormalized trajectory, one can define the topological charge only statistically [20]. This is not surprising as if one has only incomplete information about a system one usually cannot specify the value of an observable but only a probability distribution of it. In the present case this means that one has to interpolate the lattice fields in all possible ways compatible with the RG transformation and count each interpolation with its Boltzmann weight. In this way one can define a probability distribution for the

topological charge on each lattice.

If the lattice configuration is sufficiently smooth this probability distribution is sharply peaked around a certain value of the charge and we can assign this charge to the lattice configuration. Unfortunately Monte Carlo generated configurations at typical values of the coupling are not smooth enough to do this. It is not surprising then, that it is highly nontrivial to measure the charge on these configurations. For instance the geometric method, which measures the second Chern number of an interpolated continuum fiber bundle, gives an integer for any configuration but on these rough configurations this integer does not have much to do with the topological charge. We would like to emphasize that this problem is independent of the scale invariance or non-invariance of the action we discussed in Section 2.1. It is present even for FP actions. Rather this problem is the consequence of the fact that the geometric method was designed to work only on smooth configurations where the charge probability distribution is sufficiently peaked around an integer and it makes sense to say that this is *the* charge of the given configuration.

In this work we use a classically and 1-loop perfect FP action, therefore the inverse blocking procedure described in Section 2.2 defines a unique interpolation to a smoother lattice field with half the lattice spacing of the original lattice. The charge of the interpolating field can be assigned as the charge of the original rough field. As we shall see later, in our case after one step of inverse blocking the configuration becomes smooth enough that a unique integer topological charge can be defined using either the geometric method or some improved algebraic operator.

In our earlier work we had measured topological charge using the geometric definition[15, 21] on the fine configuration. This definition of the charge always gives an integer value and has no perturbative corrections [15].

An alternative “algebraic” approach to measure the topological charge is to introduce a lattice operator $q_a(x)$ which reduces to the continuum charge operator $F\tilde{F}$ for smooth lattice configurations. The topological susceptibility measured with this operator on the lattice will receive both a multiplicative and an additive renormalization constant [22]. The connection between the two methods has been recently discussed by Rastelli, Rossi, and Vicari [23]. In a recent series of papers a non-perturbative method was proposed to evaluate these renormalization constants [24].

We prefer the geometric definition as it is free of the renormalization constants. However, measuring the geometric charge is a very expensive computational bottleneck. Our goal was to find an algebraic definition which reproduces the results of the geometric charge of the inverse blocked fine configuration on

typical configurations.

We found such an algebraic charge operator by the following procedure: We generated a set of “typical” configurations and inverse-blocked them. We measured the geometric charge on the inverse blocked configurations, as well as the expectation values of several pseudoscalar operators. These operators were all simple closed loops summed over all possible orientations, with a sign (plus for even, minus for odd parity transformations of a certain reference loop) to ensure that the operator was pseudoscalar. We then did a least-squares fit to a set of coefficients c_j for a set of operators O_j , minimizing the chi-squared function

$$\chi^2 = \sum_n \left| \sum_j c_j O_j(n) - Q(n) \right|^2. \quad (4)$$

where the outer summation is over the different configurations and $Q(n)$ is the corresponding geometric charge. This procedure is similar in the spirit of the work of Ref. [24]: we are choosing a linear combination of operators whose multiplicative renormalization factor is effectively unity, as we are using the geometric charge as a fiducial. Were we to change to a very different gauge coupling, and perhaps to a different gauge group, this procedure would have to be repeated.

We found a good fit with two operators in two representations

$$q_a(x) = \sum_j c_j^1 \text{Tr}(1 - U_j) + c_j^2 (\text{Tr}(1 - U_j))^2 \quad (5)$$

with operator 1 the path $(x, y, z, -y, -x, t, x, -t, -x, -z)$ and operator 2 the path $(x, y, z, -x, t, -z, x, -t, -x, -y)$, summed over all permutations and reflections. The coupling coefficients are given in Table 3.

Table 3: Couplings of the few-parameter algebraic charge operator for SU(2) pure gauge theory.

operator	c_1	c_2
1	.09030	.48846
2	-.17863	.41270

We generated our charge operator using typical Monte Carlo configurations. Fig. 3 shows how this operator works on a set of very smooth single-instanton configurations. We overlay on this figure the charge as determined by the geometric method. Since we use this charge operator on the inverse blocked configurations where the instantons are always larger than about twice the lattice spacing, the improved algebraic charge deviates from the geometric charge by no more than a few per cent.

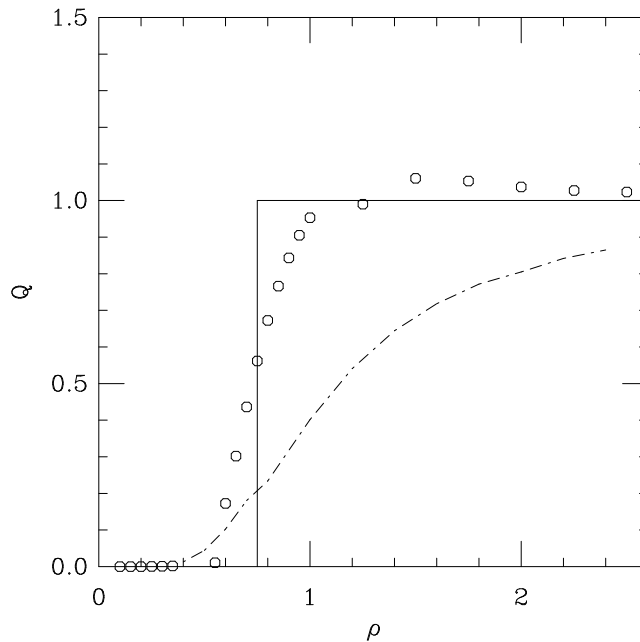


Figure 3: Topological charge vs. instanton radius from our algebraic charge operator, measured on a set of smooth instanton configurations. The step function is the geometric charge on the same configurations. The long-short dashed line shows the topological charge measured using the naive definition.

We also show on this figure the topological charge for the same set of smooth configurations, measured using the “naive” twisted plaquette $(x, y, -x, -y, z, t, -z, -t)$ loops. Over the range of the plot, it shows a marked variation with the instanton radius which can be removed by an overall multiplicative rescaling $Z(\beta)$ factor only in an average sense.

We have so far been unsuccessful in constructing an algebraic topological charge operator which does not involve inverse blocking as an intermediate step.

2.3 Controlled Smoothing

A natural way to measure topological properties of the lattice vacuum would be to inverse block several times, producing a fine interpolation with lattice spacing $(1/2)^n$ of the original coarse lattice spacing. This program has been carried out for two dimensional spin models, but the growth of the number of variables in a four dimensional inverse blocking transformation prevents us from making more than one level of inverse blocking. Instead, we adopt the following smoothing procedure:

We first inverse block a coarse lattice to a fine lattice. During this step, the action density falls by about a factor of 32, a factor of 16 because of the increase of the volume and an additional factor of about 2 because the kernel κT in Eqn. 2 picks up about half of the original action. Typical values for the action density in our simulation are $s_{coarse} = 0.9 - 1.0$ and $s_{fine} = 0.02 - 0.03$ out of a maximum value of 2. Speaking very naively, this fine action density corresponds to a very large ($O(10)$) effective gauge coupling. If we do a block transformation on a *typical* configuration generated at some β value, the blocked lattice will correspond to a $\beta_{eff} \approx \beta - \Delta\beta$ where $\Delta\beta = 4N_c\beta_0 \ln 2 = 0.257$, ($\beta_0 = 11N/(48\pi^2)$, $N_c = 2$) is given by the continuum β function of the model. Starting with a large β configuration the shift $\Delta\beta$ will have very little effect on the action density; one expects $s_{blocked} \sim 0.03$. On the other hand we know that the fine lattice blocks back to the original coarse lattice with $s_{coarse} \sim 1.0$. This is due to a very delicate cancellation and is true only if we block with the same blocking kernel and define the block links in the same way as for the inverse block transformation. The sites of the original coarse lattice correspond to a sublattice of the inverse blocked fine configuration, in our notation the all-even sublattices, i.e. to sites with all coordinates even. We have to perform the block transformation on the fine lattice with the original blocking kernel and blocked links originating from the all-even sublattice, to get back the coarse configuration. If we do the block transformation with a different blocking kernel and/or based on a different sublattice, these cancellations will not be present, and the resulting blocked lattice could be thought of as corresponding to a large β with action density of about $s_{block} \sim 0.03$.

However, to think of the smoothing as merely replacing the coarse lattice by a fine lattice with a configuration characteristic of very large beta is incorrect. On scales larger than the original coarse lattice spacing, the fine lattice retains all the structure of the coarse lattice. Only short range fluctuations have been smoothed. Since the basic assumption behind RGT is that a block transformation does not change long distance behavior, the physical properties of the blocked lattice should be the same as the fine lattice and consequently the same as the original coarse lattice independent of the choice of block transformation

and sublattice. This is true for topological objects as blocking does not create or destroy instantons larger than some critical size $\rho_c \sim a$.

With this inverse blocking/blocking procedure we map an original coarse lattice to a lattice of same size and identical long distance and topological properties but with greatly reduced action density. The sequence can be repeated and with each step the action density decreases and the resulting configuration becomes smoother.

We will refer to a blocking-inverse-blocking step as a “cycle”. (The first cycle in a sequence is just an inverse blocking step.) At the end of each cycle, we have a smooth lattice, on which we can perform measurements.

In practice, we take our blocking kernel to be the same as the inverse blocking kernel but with $\kappa = \infty$ to reduce fluctuations and build the blocked links starting from all-odd ((1,1,1,1), etc.) lattice points. In each inverse blocking step the minimization is done to a precision of less than 1% of the action of an instanton. With this precision one cycle takes about the equivalent (in CPU time) of 15-50 Monte Carlo sweeps with our gauge action on the coarse lattice. As the cycling proceeds and the configuration gets smoother the minimization typically becomes faster. This very precise minimization is probably unnecessary. Preliminary results indicate that it might be sufficient to minimize to the accuracy of about 1% of the lattice action only. On many times cycled configurations where the action is dominated by the instantons it does not make much of a difference, but on rough configurations considerable computer time can be saved by the relaxed minimization condition.

2.4 Properties of the Smoothed Configurations

As we argued in the previous section, we expect that the many times cycled configurations have the same physical properties as the original coarse configuration. In this section we study this problem in more detail.

To illustrate the effect of smoothing cycles, Fig. 5 shows the action vs. cycle number for a typical $\beta = 1.5$ configuration. This particular configuration has 3 instantons and 2 anti-instanton so the smallest its action can be is about $S = S_I(A + I) \sim 200$ (assuming the interaction between instantons is small). The topological charge and the location of the individual instantons (identified as we describe in Section 2.5) do not change during the cycling transformation.

On most configurations we did 9 cycle steps. We measured the topological charge using the algebraic operator described in Section 2.2 after each cycle.

Occasionally the total charge changed by one signaling the loss of an instanton or anti-instanton. That is not surprising as instantons that are centered differently on the lattice have slightly different critical radius [11]. During a cycling transformation the centers of the instantons are shifted and small instantons could become unstable. In practice it happens only for radius $\rho < a$ and it is consistent with the fact that our instanton identifying algorithm misses instantons with $\rho < \rho_c \sim a$. Opposite charged pairs are also stable under the cycling transformation unless their centers are closer than about 80% of the sum of their radii. We demonstrate this in Fig. 4 which shows how the charge profile of an ideal I-A pair evolves through smoothing.

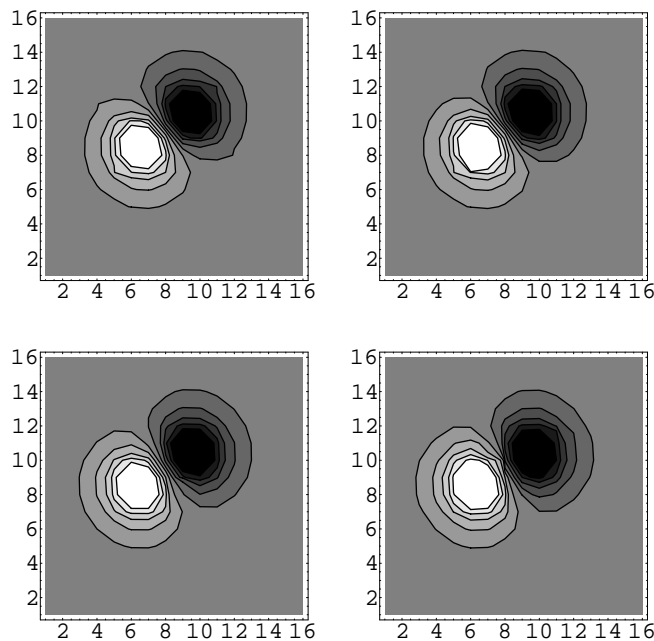


Figure 4: The evolution of the charge density profile of an ideal I-A pair both having a radius of $\rho = 1.5$ with their centers 2.5 lattice spacings apart. These snapshots were taken at smoothing step 1,2,6 and 9, always on the inverse blocked lattice.

Next we turn our attention to the static potential. While the cycling transformation does not change the long distance properties of the system, it influences the short distance behavior. The more cycling we do, the more disturbance we will see at short distance. Therefore we expect the string tension to stay constant but the Coulomb part of the potential can change.

The potential measurement involves one technical point: The subtle cancellations on the fine lattice that explain the factor of 32 drop in the action density after an inverse blocking step create a "staggered" structure on the fine lattice. While the mass gap (exponential falloff of correlators) is the same on and between different sublattices, the amplitude or overall scale factor in front of the exponential will be different for correlation functions of fine variables which are not members of the same sublattices. For example, the potential obtained from Wilson loops with length even in all directions has a different amplitude than the potential obtained from Wilson loops with odd length though the exponential fall-off for both correlators is the same. Mixing different correlators will produce inconsistent, incorrect results. To avoid the problem one must only combine correlators of fine variables which occupy a common sublattice. In this paper we only present measurements of the string tension between points of the fine lattice which belong to the same sublattice, and we average our measurements over all 16 sublattices.

The results we present in the following were obtained on 16^4 lattices at $\beta = 1.5$.

Fig. 6 shows the static potential on the original coarse lattice, and then measured on once inverse blocked lattices. For the latter data set, distances and potentials are measured in units of the coarse lattice spacing (units of two fine lattice spacings). While the potential on the inverse blocked lattice is distorted at small lattice spacing, the string tension is clearly unchanged. A fit confirms what the eye can see—the string tension is unchanged but the short distance Coulomb part is different.

On many times cycled configurations we expect the short distance distortion to increase up to the point that on our relatively small lattices the string tension will be distorted as well. To test this, we measured how the heavy quark potential changes with the number of smoothing cycles. Figure 7 shows our results obtained on the inverse blocked 16^4 configurations at cycle number 1,3,5 and 9. (We got exactly the same results by doing the measurement in each cycle on the blocked 8^4 lattices.)

As expected, the behavior of the potential on length scales of the order of the lattice spacing changes considerable over the cycles, in particular the Coulomb term is already quite suppressed on the once inverse blocked configurations. On

the other hand, the string tension, the (constant) slope of the potential at large distance, does not change at all until after about four cycles, when it starts to drop by a few per cent in each cycle. This is due to the fact that at this point the effect of smoothing starts to propagate into the distance scale on which the string tension is measured. We believe that were we able to measure the true asymptotic string tension, we would not notice any change in that.

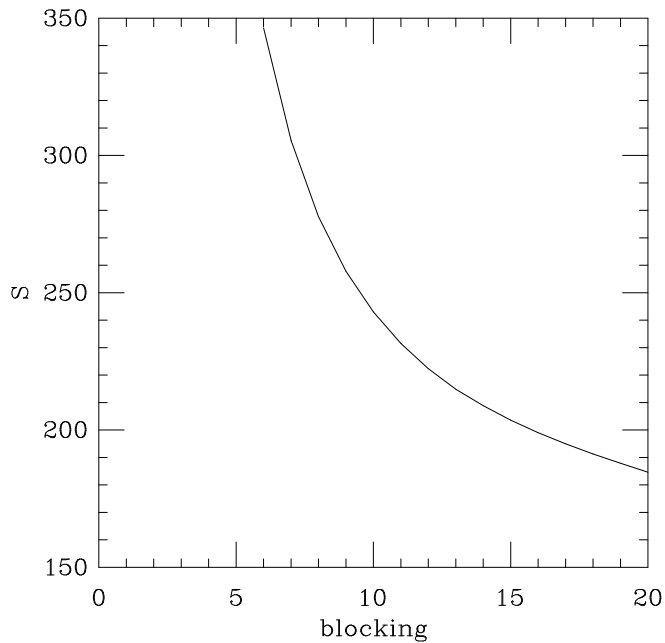


Figure 5: Action vs. cycle number for a typical lattice.

Recently Feurstein et al. [28] used a similar smoothing procedure, although they performed the Monte Carlo updates on the fine lattice and then blocked and inverse blocked the configurations. They concluded that one step of blocking and inverse blocking changed the string tension by 10-25%, depending on the value of β . The reason of the discrepancy between our results and theirs might be that they did not distinguish the inequivalent sublattices on the inverse blocked

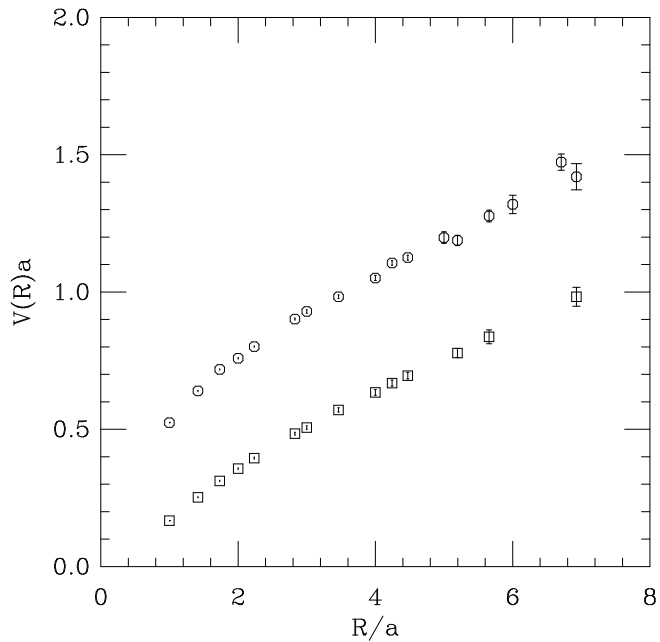


Figure 6: Potential measured on once-inverse-blocked configurations (squares), compared to standard measurements on the original lattices (octagons), for $\beta = 1.5$.

configurations.

Thus we conclude that cycling preserves long distance physics as well as the topological properties of lattice configurations, while smoothing out short distance fluctuations.

One should contrast this situation with the smoothing method known as “cooling,” [25] in which lattice configurations are brought into equilibrium at very large (or infinite) β , with the idea that the short distance fluctuations smooth away first, leaving long distance structure behind. While in principle,

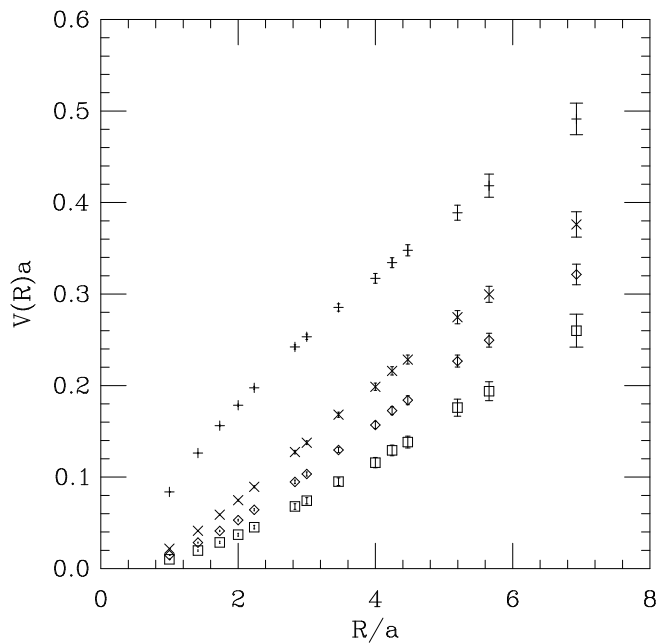


Figure 7: Potential measured on the inverse blocked 16^4 $\beta = 1.5$ configurations after performing different numbers of smoothing cycles (plusses 1 cycle, crosses 3 cycles, diamonds 5 cycles and squares 9 cycles).

because it is a local algorithm, cooling preserves the long distance structure of a configuration, in practice the number of cooling steps required to smooth the configuration enough to see instantons washes away the string tension [26]. Also, unless it is done carefully [27], cooling distorts the properties of the instantons as it proceeds, and the net topological charge of a configuration can be altered by cooling.

2.5 Identifying Instantons

We identified instantons by looking at the charge density measured with our four-parameter algebraic operator on the inverse blocked fine lattice. We were looking for peaks of the charge density that had a density profile close to that of a single lattice instanton. There is in principle some arbitrariness in the identification of instantons. If an instanton-anti-instanton pair is brought closer and closer to one another eventually the positive and negative charges cancel and nothing is left. However, this happens smoothly and there is no obvious boundary between the instanton-anti-instanton configuration and the perturbative sector. Also instantons occurring in real configurations are excited ones with shapes different from an ideal instanton profile. These problems are enhanced by the fact that as we have already explained, at presently used lattice spacings the configurations are rather rough. As an illustration we show the charge density in a two-dimensional section of one of our once inverse blocked configurations (Fig. 8a). Clearly there is no obvious way to identify “lumps” in this configuration. Note that this is a once inverse blocked configuration which is already smooth enough that the total topological charge is well defined. We found that 4-9 cycling steps (depending on the roughness of the original configuration) was sufficient to smooth the configurations so that individual instantons could be identified (Fig. 8b-d).

To identify instantons we used two different methods and checked their consistency. The first one was to look for the largest peaks in the charge density. After a peak was found we measured the average charge contained in spherical shells centered on the peak. Shells of radius up to 2-3 lattice spacings were used. The charge profile obtained in this way was compared to that of a set of discretized lattice instantons with different radii and from this the radius was inferred. If the charge profile was not consistent within 5% with the perfect instanton profile the peak was dropped. Also if a new peak was found closer than the radius of an already identified instanton, it was not counted as a separate instanton. Objects that survived these cuts were identified as instantons and their charge density was subtracted from the configuration before repeating the procedure.

According to the second procedure we computed the charge in spherical shells as above but around each lattice point. Then for each site the charge profile around it was fitted to a (lattice corrected) ideal instanton profile and the radius was computed from the fit. The fit was done pretending that there was an instanton center at the given site. Of course for most of the sites the fit was poor and the obtained radius very large. However for lattice sites closer and closer to instanton centers the fit improved and also the obtained radius got smaller. It is easy to see that the local minima of the fitted radius correspond

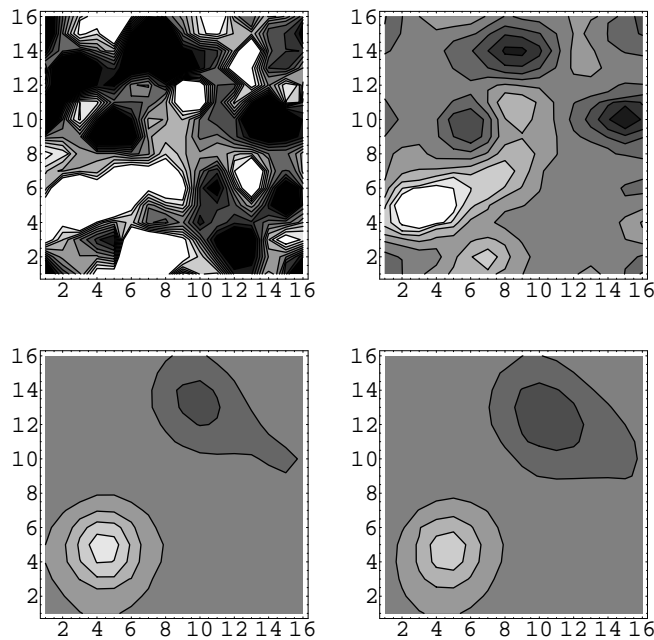


Figure 8: The topological charge density in a two-dimensional section of a typical configuration at $\beta = 1.5$ after 1,2,6 and 9 smoothing steps.

to the actual peaks; if the given site is a bit off the peak, the charge density is smaller and its average variation between spherical shells of different size is slower and this results in a larger fitted radius. The local *minima* of the radius computed in this way identified instanton centers very well. This seemingly awkward procedure was designed to work on very noisy configurations; for each lattice site we collect information from many nearby sites and local fluctuations could not deceive the algorithm.

To separate topological objects from spurious peaks that came mainly from different parts of the same large instanton we implemented further consistency checks and cuts. If two peaks were closer than the radius of the larger one, we

dropped the one that had a smaller net charge within a given radius (typically 2-3 lattice spacings). If the total charge within a radius of 2-3 lattice spacing around the peak was less than 50% of the corresponding quantity for an ideal instanton of the same size, the peak was discarded.

The apparently arbitrary parameters of our “cuts” in both methods were adjusted by looking at graphs of the charge density distribution for about ten configurations at each β , identifying the instantons “by eye” and making sure that the results given by both of the instanton finder algorithms were the same. The accuracy of the method can also be checked using the topological susceptibility defined as

$$\chi_t = \frac{\langle Q^2 \rangle}{V}, \quad (6)$$

where Q is the total charge in a volume V . The total charge can be measured using the improved charge operator and the susceptibility can be computed directly. On the other hand the charge of each configuration can also be computed as the number of instantons minus anti-instantons found by our algorithm. For $\beta = 1.5(1.6)$ calculating $Q = I - A$ gives $\chi_t = 7.5(8)10^{-4}(3.3(3)10^{-4})$ while from the total charge measurement we get $\chi_t = 7.0(8)10^{-4}(3.5(3)10^{-4})$. This shows that the instanton finder algorithm works well and within the error bars it gives the correct susceptibility.

On each configuration we performed 9 cycling steps. As we have already mentioned our smoothing algorithm left both the location and the radius of an ideal lattice instanton unchanged to a very high degree of accuracy. This was not always true for real lattice instantons generated with our Monte Carlo. While their locations were quite stable from the stage where we could reliably identify them, the size of some of the instantons kept changing slowly throughout the iteration. This change of size was less than 20% during 9 cycling steps for most of the objects, and in most cases the instantons grew. To account for this, we identified the same lumps from cycling step 6 to step 9 of the iteration and linearly extrapolated their sizes back to cycling step 1. Objects whose size changed more than 20% usually did not have an ideal instanton profile and often disappeared after repeated cycling. For these reasons they are more likely to be quantum fluctuations and not topological objects, and therefore we dropped them from the instanton count.

3 Results

3.1 Parameters of simulations

We used the static potential to set the physical scale of our action. We performed measurements at β values 1.4, 1.5 and 1.6. On $12^3 \times 16$ lattices we collected 100-300 measurements of Wilson loops (spaced five update sweeps apart) per coupling. The data was fitted using the techniques of Ref. [29] to the static potential $V(r)$ to the form

$$V(r) = V_0 + \sigma r - E/r \quad (7)$$

In Table 4 we show the results of the fit together with the Sommer [30] parameter r_0 ($r_0^2 dV(r_0)/dr = -1.65$) and we also present the lattice spacing at the different β values obtained from setting the Sommer parameter to its real-world value $r_0 = 0.5$ fm.

Unfortunately at $\beta = 1.4$ the configurations were too rough to measure the string tension and the Sommer parameter directly on the Monte Carlo generated lattices. Therefore we measured these parameters on the same set of 16^4 $\beta = 1.4$ once inverse blocked configurations that we also used for the measurement of the topological charge. This was done in exactly the same way as was described in section 2.3, distinguishing the different sublattices of the fine configurations.

Since the inverse blocked lattices correspond to lattice spacing one half of the original lattice and the fluctuations are greatly suppressed, we were able to get reliable fits even at relatively large distances and spatial separations. We measured the potential this way at $\beta = 1.5$ and 1.6 as well. At $\beta = 1.5$ the results were consistent with the direct calculation. At $\beta = 1.6$ the 8^4 lattices showed finite size effects.

Table 4: Parameters of the static potential from Wilson loops at different values of β . σ is the string tension, r_{min} and r_{max} specify the range where the potential was fitted and $r_0 = 0.5$ fm is the Sommer parameter.

FP action					
β	$a^2\sigma$	r_0/a	r_{min}	r_{max}	a (fm)
1.4	0.216(90)	2.66(3)	1.41	4.24	0.188(3)
1.5	0.122(10)	3.48(2)	1.73	10.39	0.144(1)
1.6	0.078(4)	4.30(5)	1.73	10.39	0.116(2)

3.2 Size distribution of instantons and the topological susceptibility

The size distribution of instantons in the dilute instanton gas approximation was calculated in the pioneering paper of 't Hooft [31]

$$n(\rho) = \frac{C_N}{\rho^5} \left(\frac{4\pi^2}{g^2}\right)^{2N} e^{-S_I(g^2)} \quad (8)$$

where $n(\rho)d\rho$ is the number of instantons and anti-instanton with radius between ρ and $\rho + d\rho$, C_N is a regularization dependent constant and $S_I(g^2)$ is the instanton action with the running coupling which at the one loop level reads

$$S_I(g^2(\rho)) = \frac{8\pi^2}{g^2(a)} - \frac{11}{3}N_c \ln(\rho/a). \quad (9)$$

For small radius, where this formula is applicable, $n(\rho)$ increases as a power, $n(\rho) \sim \rho^{11N_c/3-5}$. For large radius instantons the dilute gas and the perturbative approximation break down and instanton interaction effects will modify $n(\rho)$. One expects that large instantons are strongly (possibly exponentially) suppressed in the QCD vacuum but the mechanism of this suppression is not clear.

We have measured the instanton size distribution on 8^4 lattices at $\beta = 1.4, 1.5$ and 1.6 as described in Section 2.5. The parameters of our data sets are given in Table 5. The configurations were separated with 40 Monte Carlo sweeps in each case. In order to compare different β values we present the results in physical units using for the lattice spacing on the original coarse lattice the values quoted in Table 4.

Table 5: Parameters of the data sets from which topological quantities were measured. L is the lattice size (in lattice units) and a is the lattice spacing in fm, from string tension measurements.

FP action				
β	L	a , fm	La , fm	number of configurations
1.4	8	0.188	1.50	84
1.5	8	0.144	1.15	132
1.6	8	0.116	0.93	213

In Fig. 9 we present the integrated size distribution

$$N(\rho) = \frac{1}{V} \int_{\rho-\delta\rho/2}^{\rho+\delta\rho/2} n(\rho)d\rho \quad (10)$$

where V is the volume in fm^4 and

$$\int_0^\infty n(\rho)d\rho = I + A, \quad (11)$$

the total number of instantons and anti-instanton on the lattice. We chose $\delta\rho = 0.05$ fm for all 3 β values and chose the bins such that the third bin corresponded to $(1.2a, 1.2a + 0.05)$ fm. The reason for this choice is to separate regions where our instanton finding algorithm is reliable ($\rho > a$) from the region where we probably lose instantons. With the above binning the third bin has all the physical instantons while the second bin misses some small radius instantons and the first bin is almost empty.

In addition to the cutoff effects the instanton distribution is distorted by finite volume effects as well. As large instantons will not fit into small volumes, $N(\rho)$ will be affected for large ρ , especially for larger β values.

If the instanton distribution scales, the results for the 3 different β values should form a universal curve, at least in the region where finite cutoff and finite volume effects are negligible. In Fig. 9 we indeed see such a universal curve. The third bins for $\beta = 1.4$ and 1.5 follow this universal curve and that makes us trust the third bin of the $\beta = 1.6$ curve predicting that the density curve peaks around $\rho \approx 0.2$ fm. For large ρ values the $\beta = 1.6$ curve separates around $\rho \geq 0.3$ fm and we might observe the $\beta = 1.5$ curve separating at around $\rho \geq 0.4$ fm. Combining the three β values we can map the density distribution for $0.15 \text{ fm} < \rho < 0.5 \text{ fm}$ which includes most of the interesting region. It would be informative to go below $\rho = 0.15$ fm but for that the calculation has to be repeated at larger beta values and on larger lattices. This is not an impossible task, but not a workstation project either.

We expected our instanton finding algorithm to lose instantons with $\rho < a$ and our results are consistent with this expectation. Other instanton finding algorithms can have different thresholds. For example the improved cooling method of Ref. [6] is claimed to keep instantons above $\rho = 2.3a$. This cutoff is about twice ours. If the simulations are performed at $a \approx 0.12$ fm, only instantons larger than $\rho_{min} \approx 0.3$ fm would be counted. This value is well above the peak of the instanton distribution we found in our simulation. In Ref. [6] the distribution peak was found at around $\rho_{peak} \approx 0.45$ fm. In light of the above discussion it is most likely an artificial peak due to the large ρ_{cut} of the instanton algorithm.

The topological susceptibility can be easily calculated from our data. We use the usual definition for the susceptibility

$$\chi_t = \int d^4x \langle q(x)q(0) \rangle \quad (12)$$

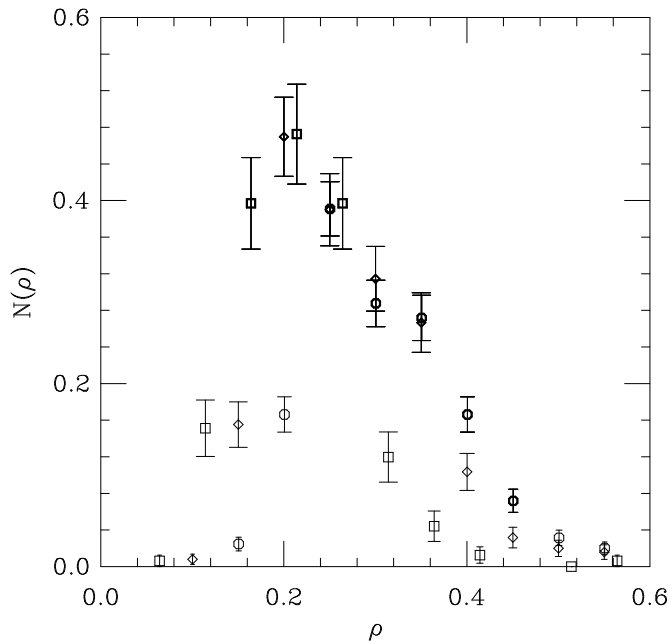


Figure 9: The density distribution of instantons. Data at $\beta = 1.6$ are given by squares, $\beta = 1.5$ diamonds, and $\beta = 1.4$ octagons. The bold data points are ones for which the instanton radius is large compared to the lattice spacing and small compared to the simulation volume.

or

$$\chi_t = \frac{\langle Q^2 \rangle}{V} \quad (13)$$

where Q is the topological charge of the configuration in volume V . We do not deal here with the problem of connecting this Euclidean definition to the Witten-Veneziano formula but we do expect χ_t to show scaling.

We quote the result obtained by measuring the total charge of the configurations using our algebraic operator $\beta = 1.5$. At $\beta = 1.4$ we lose small instantons

due to the larger lattice spacing, and at $\beta = 1.6$ we are missing the large instantons in the simulation. It is possible to combine the three curves but the result changes very little:

$$\chi_t = 0.11(1)r_0^4 = 230(30) \text{ MeV} \quad (14)$$

This number is consistent with the result we obtained using the FP action in Ref [12] but it is about 20% larger than the quoted susceptibility in [6]. Based on the analysis above this discrepancy is not surprising. Indeed, if we keep only instantons with $\rho > 0.27 \text{ fm}$ we obtain for the susceptibility $\chi_t = 190 \text{ MeV}$, in complete agreement with the value quoted in [6].

3.3 Correlations among instantons

Combining our results for the density distribution at $\beta = 1.5$ and 1.6 we find that the instanton density is $n \approx 2.0 \text{ fm}^{-4}$. With this density and average radius of about 0.2 fm the instantons are far from dense. In fact, they occupy only a small fraction, between 3% and 10% of the available space.

Do instantons develop some additional structure preventing them from growing in size (that would energetically be favorable in the dilute instanton gas)? We measured the distance between nearest objects to reveal any correlation. The following analysis was done using only the $\beta = 1.4$ configurations since these were the only ones where each lattice contained a significant number of objects ($O(10)$). In Fig. 10 we plot the distribution of the nearest like and unlike objects in addition to the distribution of the nearest objects as the function of their distance normalized by their combined radius, $R/(\rho_1 + \rho_2)$. There is no significant difference between like and unlike objects. No two objects get closer than about 80% of their combined radius indicating a repulsive core interaction. On the other hand, most objects have a neighbor within 1.2 times of their combined radius. That is significantly closer than the average distance 0.84 fm inferred from the density. That could indicate pairing or long-range, for example linear (polymer like?) structure. To distinguish the two possibilities we calculated the fraction of instantons belonging to the largest cluster on any given lattice. An instanton belongs to a cluster if it is closer to any member of the cluster than some constant c times the combined radius. We found that with $c = 1.2$ over 80% of the instantons belong to the largest cluster indicating some type of long range structure.

A similar conclusion is reached by defining the clusters as connected regions of the lattice where the charge density is greater than a given number c . Measuring c in units of the average (modulus of the) charge density we found that for $c = 2, 3, 4$, 95%, 84% and 73% of the instantons belonged to the largest

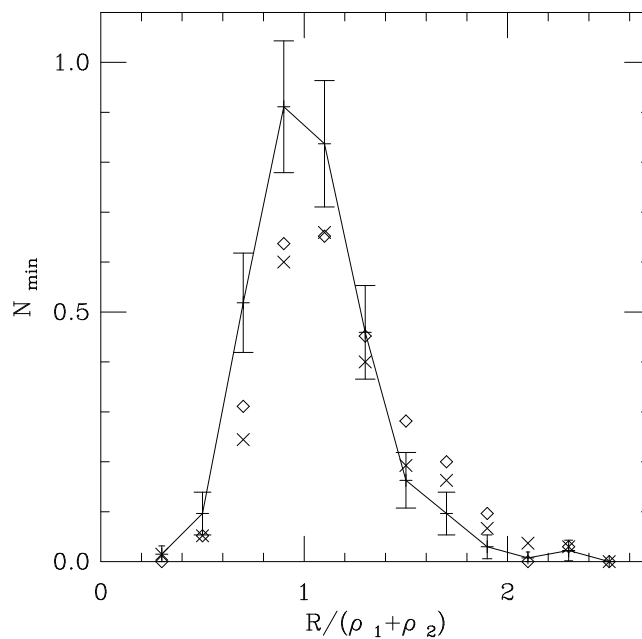


Figure 10: Distribution of nearest objects (solid line). The diamonds correspond to the distribution of nearest like-sign objects, the crosses to nearest unlike-sign objects. The error bars for the like and unlike distributions are suppressed for clarity.

cluster. These clustering properties together with the fact that instantons take up only a small fraction of the total volume show that the instanton liquid has a very peculiar structure. It is far from being close packed; rather, most of the instantons “touch” at least one neighbor and are part of a large cluster.

3.4 Instantons and confinement

It is quite remarkable that in our smoothing procedure after about nine iterations of blocking-inverse blocking, the action of the resulting lattice configurations is dominated by instantons, while the long range physics is essentially unchanged. This means that the large-scale structures that are presumably responsible for confinement are left intact by our smoothing procedure.

Since most of the leftover excitations are accounted for by instantons (at least in terms of action), it is sensible to ask whether the instantons make a substantial contribution to the heavy quark potential. It is generally believed that instantons by themselves do not produce confinement for heavy quarks (for a recent review see [2]), however most of the arguments supporting this claim use some sort of approximation (e.g. dilute instanton gas [32], mean field [1]) that might not be justifiable.

To test this, we measured the contribution of instantons to the heavy quark potential on the lattice. We generated a set of 100 artificial lattice configurations by putting together smooth lattice instantons with exactly the same sizes and locations as we found them in the real Monte Carlo generated configurations at $\beta = 1.5$. Unfortunately we did not have any information about the relative orientation of instantons in group space so in the artificially built configurations we put them all aligned. This was done by adding the vector potentials (the log of the link variables) of the smooth instantons in singular gauge. The use of singular gauge was essential for the fast enough decay of the instanton vector potentials. In this way we obtained configurations that had an action a few percent higher than the sum of the ideal individual instanton actions. This showed that our “gluing” procedure produced smooth configurations. To ensure even more smoothness we blocked these 16^4 configurations to 8^4 .

We measured the heavy quark potential on this ensemble of artificial configurations and compared it to the same quantity measured on the real Monte Carlo generated nine times smoothed 8^4 configurations. Fig. 11 shows that instantons make only a very small contribution to the large distance force between heavy quarks. Our results are in qualitative agreement with the ones obtained by Diakonov et al. [33] who computed the heavy quark potential from the instanton liquid. They found that it goes to a constant at a distance of 1-2 fm. A more quantitative comparison of our and their results is not very meaningful since we computed the potential only up to about 1 fm and also the (fixed) instanton size that they used was larger than the average size in our ensemble.

All this, however, shows that instantons by themselves cannot explain confinement, and even if they play any role in the confinement mechanism, it is

very subtle.

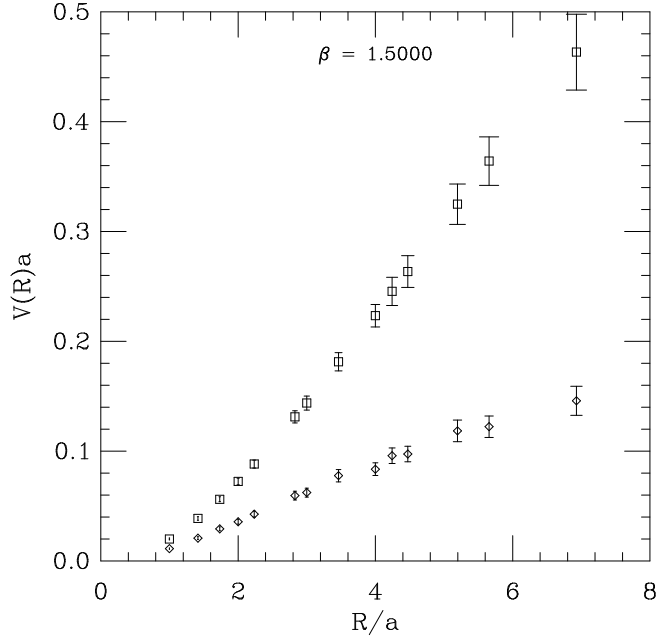


Figure 11: The heavy quark potential measured on the artificially produced instanton configurations (diamonds) and the potential measured on the corresponding 9 times smoothed “real” configurations (squares), at $\beta = 1.5$.

This might be understood qualitatively as follows. We have already seen that instantons live at a certain length scale which can be characterized by their average radius (about 0.2 fm). We expect that the effect of instantons can be felt only up to this length scale. On the other hand confinement, as described by an asymptotic string tension, is a genuinely infrared effect and the excitations responsible for it must be present at all large enough length scales. If we perform some gradual coarse graining (e.g. by blockings) at a certain point the instantons will completely disappear and their only remaining trace will be to give some modification to the effective action for the remaining large scale

fluctuations. Confinement however is expected to be still present beyond this point in the coarse graining procedure.

It follows that the excitations which can be important for confinement are very large-scale smooth objects that cost extremely little in terms of action, but nevertheless are efficient in disordering the system on large distance scales. These might be for example thick $Z(2)$ vortices [34] or some other semiclassical objects. Another recently proposed semiclassical picture of confinement is based on lumps with topological charge of $1/2$ [35]. Our analysis shows that on the smoothed configurations the topological structure consists only of charge $(-)$ 1 (anti)instantons and no half charged objects. It is therefore quite unlikely that charge $1/2$ objects play a direct role in confinement mechanism.

It would be certainly interesting to know more about the nature of excitations responsible for confinement. Our smoothing technique is well suited to the study of this question because it suppresses the ultraviolet “noise” that dominates the action on Monte Carlo generated configurations and at the same time it does not distort the large scale structure of the lattice configurations. We hope to return to this question in a future publication [36].

4 Conclusions

We have described a method for smoothing away the short-distance fluctuations from equilibrium configurations of $SU(2)$ gauge field variables. The smoothing method preserves topological charge no matter how much it is used. It also preserves the long distance structure of the field configurations, as we show explicitly by measuring the string tension. The action of the smoothed configurations is dominated by localized structures—instantons. The density and mean size of the instantons is quite consistent with the range of expectations from instanton liquid models. The mean instanton size is quite a bit smaller than previous lattice simulations of $SU(2)$ gauge theory have reported, and the topological susceptibility is larger. We believe that this disagreement with the work of others is due to the fact that our algorithm for finding topological charge can detect instantons of size comparable to one lattice spacing, while the other algorithms have much higher size thresholds.

We find a non-trivial correlation between instantons. They do not form a dilute gas nor they are closely packed; rather, they appear to clump in some difficult-to-quantify way.

As far as we can tell, instantons are not directly responsible for confinement.

Since the smoothing algorithm preserves long distance physics, we believe that it might be possible to identify the field configurations responsible for confinement by examining smoothed configurations. Exactly how that could be done remains an open problem.

Finally, having measured the size distribution and density of instantons does not tell us whether they are directly responsible for any observable physics effects. A major component of instanton phenomenology involves the interactions of instantons with fermions. A study of those interactions remains an open problem. We expect that the methods we have described here, especially combined with an inverse blocking algorithm and fixed-point action for fermions, will enable us to shed light on these questions.

Acknowledgements

We would like to thank P. Hasenfratz, F. Niedermayer and A. Sokal for useful conversations, and the Colorado High Energy experimental groups for allowing us to use their work stations. We would like to thank Matthew Wingate for helping us fit potentials. This work was supported by the U.S. Department of Energy and by the National Science Foundation.

References

- [1] D. Diakanov, Lectures at the Enrico Fermi School in Physics, Varenna, 1995, hep-ph/9602375.
- [2] T. Schäfer and E. V. Shuryak, “Instantons in QCD,” hep-ph/9610451.
- [3] S. Weinberg, Phys. Rev. D11 (1975) 3583; G. t’Hooft, Phys. Rev. D14 (1976) 3432; Phys. Rev. Lett. 37 (1976) 8.
- [4] E. Witten, Nucl. Phys. B156 (1979) 269; G. Veneziano, Nucl. Phys. B159 (1979) 213.
- [5] C. Michael and P.S. Spencer, Phys. Rev. D52 (1995) 4691.
- [6] P. de Forcrand, M. Garcia Perez and I.-O. Stamatescu, hep-lat/9701012.
- [7] P. Hasenfratz and F. Niedermayer, Nucl. Phys. B414 (1994) 785; P. Hasenfratz, Nucl. Phys. B (Proc. Suppl) 34 (1994) 3; F. Niedermayer, *ibid.*, 513.

- [8] T. DeGrand, A. Hasenfratz, P. Hasenfratz, F. Niedermayer, Nucl. Phys. B454 (1995) 587.
- [9] T. DeGrand, A. Hasenfratz, P. Hasenfratz, F. Niedermayer, Nucl. Phys. B454 (1995) 615.
- [10] A. Farchioni, P. Hasenfratz, F. Niedermayer and A. Papa, Nucl. Phys. B454 (1995) 638.
- [11] T. DeGrand, A. Hasenfratz, D. Zhu, Nucl. Phys., B475 (1996) 321.
- [12] T. DeGrand, A. Hasenfratz, D. Zhu, Nucl. Phys. B478 (1996) 349.
- [13] T. DeGrand, A. Hasenfratz, D. Zhu, Talk given at Lattice 96: 14th International Symposium on Lattice Field Theory, St. Louis, MO, 4-8 Jun 1996; Nucl. Phys. B (Proc. Supp.) 53 (1997) 945.
- [14] M. Lüscher, Nucl. Phys. B200 (1982) 61;
- [15] B. Berg, M. Lüscher, Nucl. Phys. B190 (1981) 412.
- [16] D. J. R. Pugh and M. Teper, Phys. Lett. 224B (1989) 159.
- [17] M. Göckeler, A. S. Kronfeld, M. L. Laursen, G. Schierholz, and U.-J. Wiese, Phys. Lett. 233B (1989) 192.
- [18] V. Branchina and J. Polonyi, hep-th/9606160; J. Fingberg and J. Polonyi, hep-lat/9602003.
- [19] R. Burkhalter, Phys. Rev. D54 (1996) 4121.
- [20] W. Bietenholz, R. Brower, S. Chandrasekharan and U.-J. Wiese, Nucl. Phys. B53 (Proc. Suppl.) (1997) 921; hep-lat/9704150.
- [21] M. Lüscher, Commun. Math. Phys. 85 (1982) 29; A. Phillips and D. Stone, Commun. Math. Phys. 103 (1986) 599.
- [22] M. Campostrini, A. Di Giacomo and H. Panagopoulos, Phys. Lett. B212 (1988) 206.
- [23] L. Rastelli, P. Rossi, and E. Vicari, Pisa preprint IFUP-TH 53/96; hep-lat/9610004.
- [24] A. Di Giacomo, E. Vicari, Phys. Lett. B275 (1992) 429; B. Alles, M. Campostrini, A. Di Giacomo, Y. Gündüç, and E. Vicari, Phys. Rev. D48 (1993) 2284; C. Christou, A. Di Giacomo, H. Panagopoulos and E. Vicari, Phys. Rev. D53 (1996) 2619.
- [25] D. J. R. Pugh, M. Teper, Phys. Rev. Lett. B218 (1989), 326.

- [26] M.-C. Chu, J. M. Grandy, S. Huang, and J. W. Negele, Phys. Rev. D49 (1994) 6039.
- [27] Cf. the discussion of perturbative stability of instanton solutions by M. Pérez, A. González-Arroyo, J. Snippe, and P. van Baal, Nucl. Phys. B413 (1994) 535.
- [28] M. Feurstein, E.-M. Ilgenfritz, M. Müller-Preussker and S. Thurner, Berlin preprint HUB-EP-96/59, hep-lat/9611024.
- [29] U. Heller, K. Bitar, R. Edwards, A. Kennedy, Phys. Lett. 335B, 71 (1994).
- [30] R. Sommer, Nucl. Phys. B411 (1994) 839.
- [31] G. 't Hooft, Phys. Rev. D14 (1976) 3432.
- [32] C. Callan, R. Dashen and D. Gross, Phys. Rev. D17 (1978) 2717; D18 (1978) 4684; D19 (1979) 1826.
- [33] D.I. Diakonov, V.Yu. Petrov and P.V. Pobylitsa, Phys. Lett. B226 (1989) 372.
- [34] E.T. Tomboulis, Phys. Lett. B303 (1993) 103; T.G. Kovács and E.T. Tomboulis, Nucl. Phys. B (Proc. Suppl.) 53 (1997) 509.
- [35] A. González-Arroyo and A. Montero, Nucl. Phys. B (Proc. Suppl.) 53 (1997) 596; Phys. Lett. B387 (1996) 823.
- [36] T.G. Kovács and E.T. Tomboulis, in preparation.